Journal of Power Sources 261 (2014) 206–211

Contents lists available at ScienceDirect

Journal of Power Sources

journal homepage: www.elsevier.com/locate/jpowsour

Preparation and electrochemical properties of Zr-site substituted $Li_7La_3(Zr_{2-x}M_x)O_{12}$ (M = Ta, Nb) solid electrolytes

Mian Huang [a], Mao Shoji [b], Yang Shen [a], Ce-Wen Nan [a], Hirokazu Munakata [b], Kiyoshi Kanamura [b,*]

[a] School of Materials Science and Engineering, State Key Lab of New Ceramics and Fine Processing, Tsinghua University, Beijing 100084, China
[b] Department of Applied Chemistry, Graduate School of Urban Environmental Sciences, Tokyo Metropolitan University, 1-1 Minami-Ohsawa, Hachioji, Tokyo 192-0397, Japan

HIGHLIGHTS

- $Li_7La_3Zr_2O_{12}$ (LLZ) solid electrolytes doped with Ta and Nb were prepared.
- Effects of γ-Al_2O_3 sintering aid on Ta- and Nb-doped LLZs were investigated.
- The micro-structure of Nb-doped LLZ was improved by γ-Al_2O_3 sintering aid.
- 1.23×10^{-3} S cm^{-1} was obtained for Nb-doped LLZ at 50 °C.
- All-solid-state cells using LLZTa and LLZNb worked successfully.

ARTICLE INFO

Article history:
Received 16 November 2013
Received in revised form
15 March 2014
Accepted 18 March 2014
Available online 26 March 2014

Keywords:
All-solid-state Li ion battery
Solid electrolyte
Garnet structure
Li ion conductivity
Doping

ABSTRACT

$Li_7La_3Zr_2O_{12}$ (LLZ) solid electrolytes with Zr site partially substituted by Ta and Nb elements were prepared via the conventional solid-state reaction. All the compositions could lead to the cubic garnet-type structure after sintering at 1150 °C. The use of γ-Al_2O_3 as a sintering aid in the preparation of doped LLZ was studied. It was shown that Al could help to improve the micro-structure for Nb doping, but not necessary for Ta doping. The Ta and Nb doping enhanced the ionic conductivity at 25 °C to 4.09×10^{-4} S cm^{-1} and 4.50×10^{-4} S cm^{-1}, respectively. A conductivity as high as 1.23×10^{-3} S cm^{-1} was obtained when measured at 50 °C in air for the Nb-doped LLZ. All-solid-state batteries with LLZTa and LLZNb solid electrolytes were assembled and tested. The cyclic voltammetry (CV) measurement indicated the successful working of the batteries.

1. Introduction

Lithium ion secondary battery has been one of the most promising and practical electrochemical power sources as a technical solution to today's energy problem globally. The high energy density and power density make lithium battery suitable for a wide range of applications including portable electronic devices, electrical vehicles and even stationary power storage [1–3]. However, the safety problem attracts much attention in recent years due to more and more reports on lithium ion battery inflammation or explosion incidents. The main reason for these accidents is the use of liquid electrolyte materials, which is prone to cause fire intrinsically. Therefore, substituting liquid electrolyte with solid electrolyte becomes one of the most radical solutions to solve the safety problem [4,5].

Among the many solid electrolyte materials discovered so far, $Li_7La_3Zr_2O_{12}$ (LLZ) with the garnet-type structure is a promising candidate used in all-solid-state lithium batteries, which exhibits a high stability with Li metal and wide electrochemical window [6–8]. Since its first report, a lot of work has been focused on obtaining the cubic phase which has a much higher ionic conductivity than its tetragonal phase [9–14]. The most effective method is to dope some elements during the preparation process, such as Al, Ta or Nb. And a high conductivity at room temperature could usually be obtained with the stabilization of cubic phase [15–20]. In addition, a good contact between LLZ and electrode materials is also necessary for an all-solid-state lithium battery, since the largest resistance in a cell mainly depends on the interface.

* Corresponding author. Tel./fax: +81 42 677 2828.
E-mail address: kanamura@tmu.ac.jp (K. Kanamura).

http://dx.doi.org/10.1016/j.jpowsour.2014.03.070
0378-7753/

In this work, LLZ with Ta and Nb elements doping were prepared and compared with those without doping. The effects of doping species, amounts and sintering conditions on the structure and ionic conductivity of LLZ were examined. All-solid-state battery with the configuration of Al/$LiCoO_2$/LLZ/Li/Cu was fabricated and tested with a cyclic voltammetry.

2. Experimental

All the samples were prepared via the conventional solid-state reaction. $LiOH{\cdot}H_2O$ (KANTO Chemical, 98%), $La(OH)_3$(HIGH PURITY Chemicals, 99.99%) and ZrO_2(TOHSO) were used as the raw materials. The doping elements of Ta and Nb were from their oxides, Ta_2O_5 (KANTO Chemical, 99.95%) and Nb_2O_5 (KANTO Chemical, 99.95%), respectively. The raw material $LiOH{\cdot}H_2O$ was preheated at 200 °C overnight to fully dehydrate. The starting materials were precisely weighted according to the nominal formula of $Li_7La_3Zr_{1.625}M_{0.375}O_{12}$ (M = Ta, Nb) and finely mixed by grinding for 1 h. The mixture was calcined at 900 °C for 6 h. γ-Al_2O_3 (HIGH PURITY Chemicals, 99.99%) was added to the calcined product as a sintering aid and mixed by mechanical milling with zirconia balls for 3 h. The amount of γ-Al_2O_3 was 0.15 g for every 10 g of the calcined powders. Finally, the dried powder was pressed into a pellet with a diameter of 16 mm followed by sintering at 1150 °C. To prevent the severe lithium loss during high temperature sintering, all the pellets were covered by some protective powder with the same composition.

The phase composition was characterized with X-ray diffraction (XRD, Rigaku RINT-Ultima) using Cu K_α radiation at a scanning rate of 2° min^{-1}. The cross-section morphology of the sintered samples was observed with a scanning electron microscope (SEM, JEOL JSM 6490A). The impedance data were measured with an electrochemical impedance analyzer (EIS, Solartron SI1260) in a frequency range from 10 Hz to 1 MHz under amplitude of 10 mV. Au was sputtered on both surfaces of the pellet as ion blocking electrodes. In the temperature dependence measurements from 25 °C to 50 °C, data were collected after a stabilization time of 5 min at each target temperature.

All-solid-state battery was assembled with the $LiCoO_2$ (LCO) cathode and Li metal anode. LCO sol precursor was prepared with CH_3COOLi, $Co(CH_3COO)_2{\cdot}4H_2O$, C_3H_8O, H_2O and polyvinylpyrrolidone (PVP) [8,21]. The sol precursor was coated on the LLZ surface by spin coating method followed by annealing at 700 °C for 1 h. The formation of LCO crystal was examined by Raman spectroscopy (JASCO NRS-1000) with 532 nm laser radiation. Li metal foil was pressed onto the other surface of LLZ pellet of about 0.4 mm in thickness as anode. The all-solid-state cell was aged at 60 °C overnight before the cyclic voltammetry (CV) measurement which was performed from 2.5 V to 4.5 V vs. Li/Li^+ at a scanning rate of 1 mV min^{-1}.

3. Results and discussion

3.1. Preparation and characterization of $Li_7La_3(Zr_{2-x}M_x)O_{12}$ (M = Ta, Nb)

The phase compositions of LLZ samples after sintering are shown in Fig. 1. A simulated X-ray diffraction pattern of garnet structure with the space group of *Ia*3*d* is given in the bottom for comparison. For the sample without any element doping, cubic garnet structure was obtained. This is mainly due to the use of Al_2O_3 sintering aid [6]. It was initially found that stabilization of cubic LLZ was due to the contamination of Al from crucibles during the sintering process. As an advantage of this accidental finding, alumina could be used intentionally to obtain a high ionic conductivity of LLZ, which was also performed in this work. However, an intense diffraction peak around 27.5° with the index of (400) was observed. The extraordinary peak intense was due to the orientation effect of the crystalline sample after long-time sintering. For the other element-doped LLZ samples, X-ray data were collected with their powder forms after sintering. The normal peak intensities and their relative ratios were obtained, as can be seen in Fig. 1. The cubic garnet structure remained after doping with Ta or Nb. Ta and Nb elements have the similar ionic radii with Zr, therefore these doping elements more likely enter into the Zr sites. Aiming at the same formula, the same molar ratio of doping elements was used.

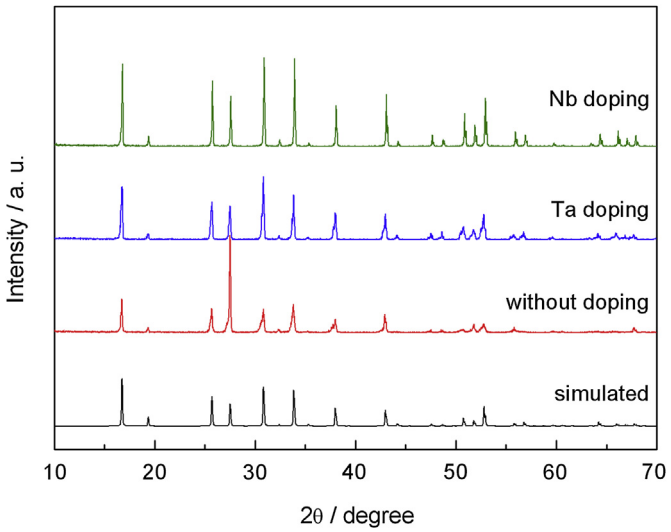

Fig. 1. XRD patterns of LLZ samples sintered at 1150 °C with Ta, Nb doping and without doping. The simulated diffraction pattern with cubic garnet structure is also shown in the bottom for a clear comparison.

The cross-sectional morphology of the sintered LLZ samples could be observed in Fig. 2. The grains were well grown with intimately connecting each other after sintering at 1150 °C. However, the pores with an average size of several micro meters existed, as shown in Fig. 2(a). This might be due to the evaporation of lithium-containing compounds and subsequent shrinkage during grain growth. Compared with the sample without doping, both Ta and Nb elements improved the sample densities. In Ta doped samples shown in Fig. 2(b), the grain growth was more developed. In the case of Nb doped sample shown in Fig. 2(d), the average pore size was much smaller than that without doping. As a result, a better sintering was obtained in both cases. In addition, there seems to be a significant difference between Ta and Nb elements during the sintering process. When sintered without Al aid in Ta doping, a dense micro structure could still be obtained, as shown in Fig. 2(c). It indicated that Ta element might also play the role of sintering aid. In the case of the sample sintered without Al aid in Nb doing, as shown in Fig. 2(e), larger pores could be clearly observed, indicating a poor sintering process. Thus, it can be concluded that Al element is necessary in Nb doping, but optional in Ta doping for a well sintered sample. The rough fracture surface may influence a heterogeneous property of the composition distribution.

The impedance spectra of Ta and Nb doped LLZ with Al aid are shown in Fig. 3. The linear data in the low frequency range are from the ion blocking Au electrodes. However, there is no obvious semi-circles up to 1 MHz in the measurements. Thus the intersection between the impedance spectrum and the real axis was used to evaluate the total conductivity. A higher sweeping frequency might help to observe the semi-circle profiles of LLZ samples, in which

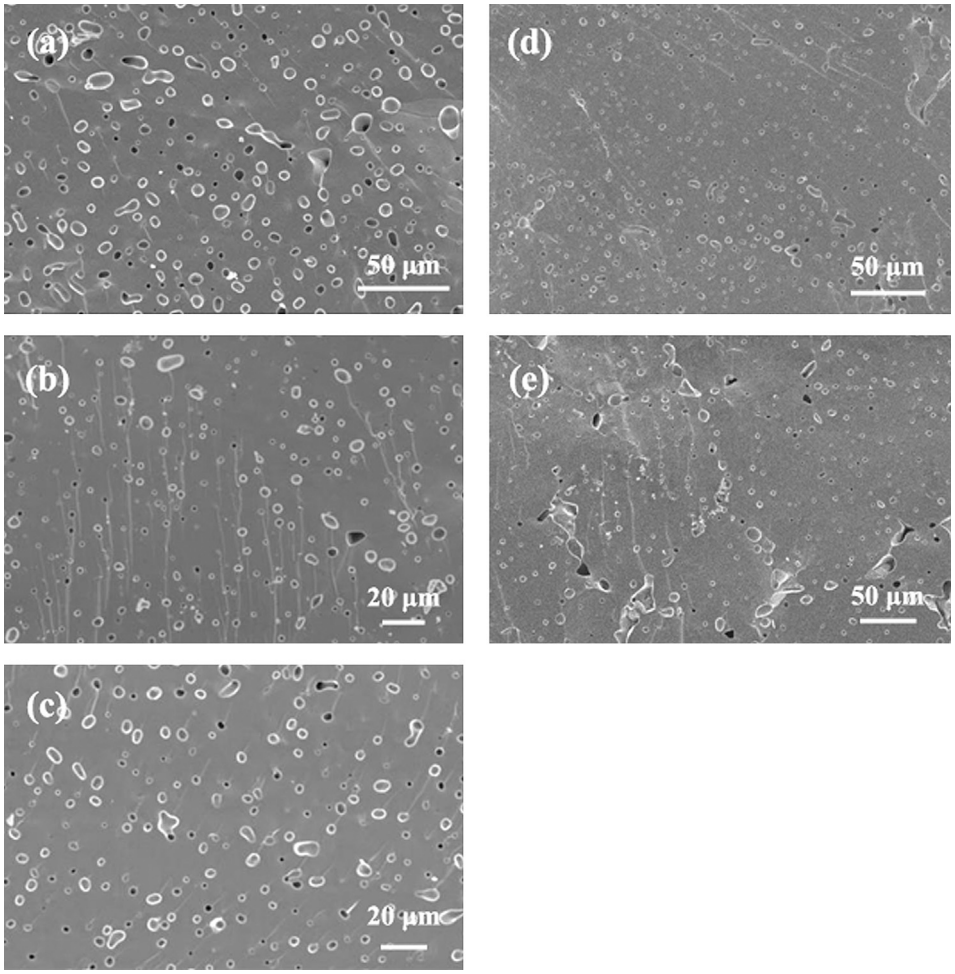

Fig. 2. Cross-sectional morphology of LLZ: (a) without doping, (b) Ta doping with Al aid, (c) Ta doping without Al aid, (d) Nb doing with Al aid and (e) Nb doping without Al aid.

case the bulk and grain boundary conductivities could be separately obtained.

The ionic conductivity as a function of temperature for LLZ samples are shown in Fig. 4. The conductivity data of Ta and Nb doped LLZ samples are from those prepared with Al aid. The measurements were performed from 25 °C to 50 °C, and all the data agreed well with the Arrhenius relation between conductivity and temperature. At 25 °C, LLZ sample without doping exhibited a conductivity of 1.11×10^{-4} S cm^{-1}. And it was greatly enhanced by Ta and Nb doping, achieving 3.11×10^{-4} S cm^{-1} and 3.81×10^{-4} S cm^{-1}, respectively. LLZ without doping and Nb doped

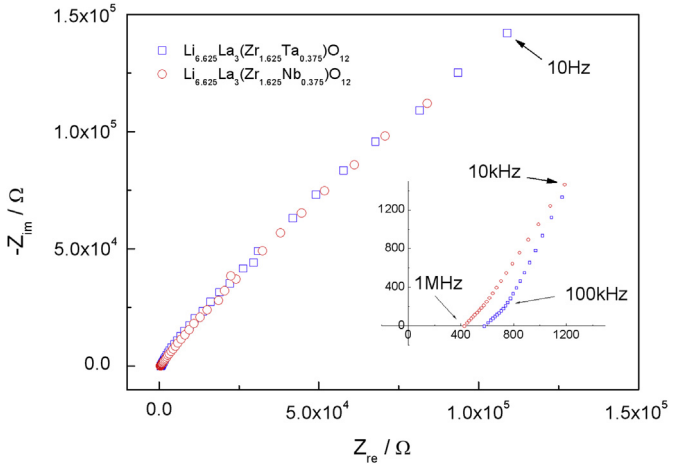

Fig. 3. Impedance spectra of Ta and Nb doped LLZ measured at 25 °C.

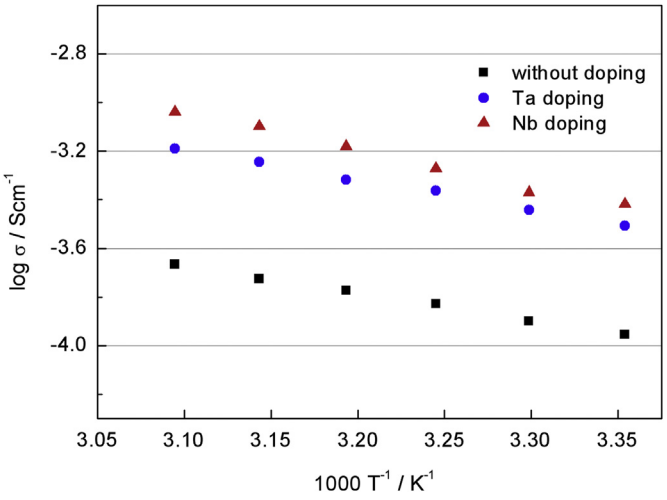

Fig. 4. Arrhenius plot of LLZ with different doping conditions measured from 25 °C to 50 °C in air.

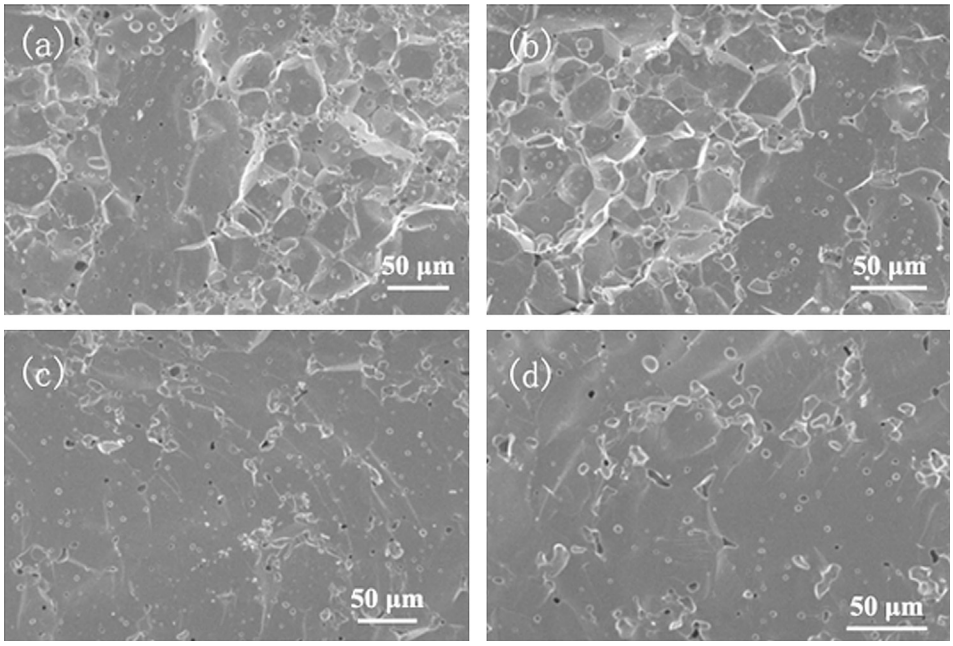

Fig. 5. Micro-structural evolution of Ta doped LLZ as a function of sintering duration time: (a) 12 h, (b) 18 h, (c) 24 h and (d) 30 h.

sample shared the same activation energy of 0.31 eV, which was decreased to 0.24 eV by Ta doping.

In order to further improve the conductivity of Ta doped LLZ, the effect of sintering duration time on the structural and conductive properties was investigated. The micro-structural evolution of Ta doped LLZ as a function of sintering duration time could be seen in Fig. 5. When the sintering duration time was short, for example, for 12 h and 18 h, crystalline grains with the polyhedral shape could be observed. Typically, the grains were in the size of tens of micro meters. Although some micro-pores appeared at this stage, the grains connected each other tightly, benefiting the further grain growth. After prolonging the sintering duration time to 24 h and 30 h, small crystalline grains disappeared and quite larger grain bulk formed. At the same time, the micro-pores became large, and gathered along the grain boundaries especially. It is notable that, the interfaces especially as grain boundaries in the sintered LLZ samples play an important and practical role for the total conductivity. Usually, large grains might be beneficial for the bulk Li^+ ion conduction. Therefore, the property of grain boundaries, such as volume fraction of pores and/or connectivity of grains, may make a difference in the samples under different sintering duration time.

Accordingly, the conductivities of the Ta-doped LLZ with Al aid sintered for different duration time are shown in Fig. 6. The sample sintered for 36 h is added for comparison. It is obviously observed that the conductivity was enhanced with reducing the sintering duration time. The highest conductivity at 25 °C was 4.09×10^{-4} S cm^{-1} with the sample sintered for 12 h. However, the activation energy of 0.30 eV was slightly higher than that sintered for 36 h. One of the possible reasons for this enhancement of conductivity by reducing the sintering duration time could be the micro-structural difference. In the case of shorter sintering time, smaller grains were grown, and the grain boundaries were well developed, which were beneficial for the Li^+ ion conduction. However, the larger pores especially along the grain boundaries, in the case of longer sintering duration time, would cause large resistance for the ionic conduction. In addition, more lithium would

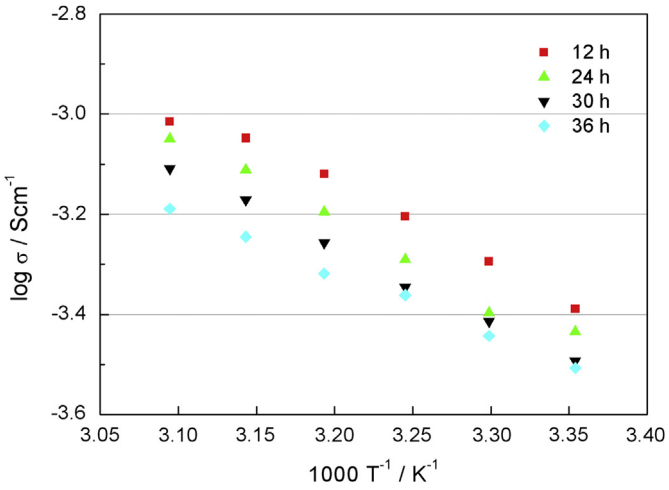

Fig. 6. Arrhenius plot of Ta doped LLZ sintered for different duration time.

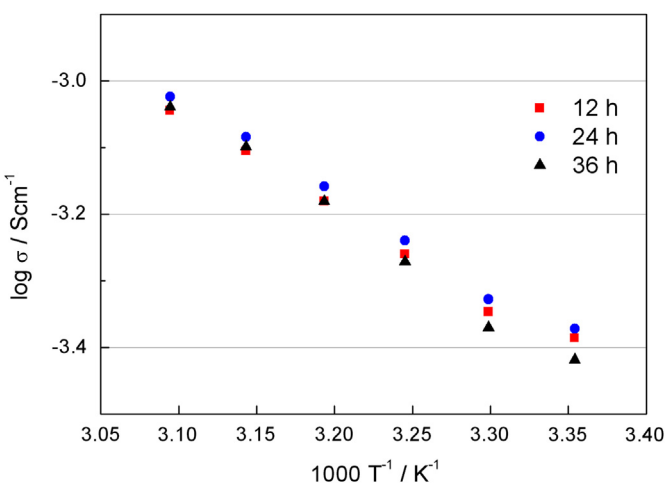

Fig. 7. Arrhenius plot of Nb doped LLZ sintered for different duration time.

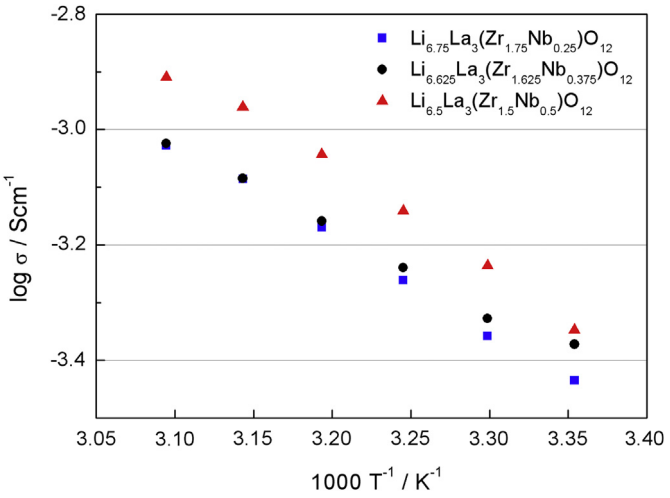

Fig. 8. Arrhenius plot of Nb doped LLZ with different Nb doping content.

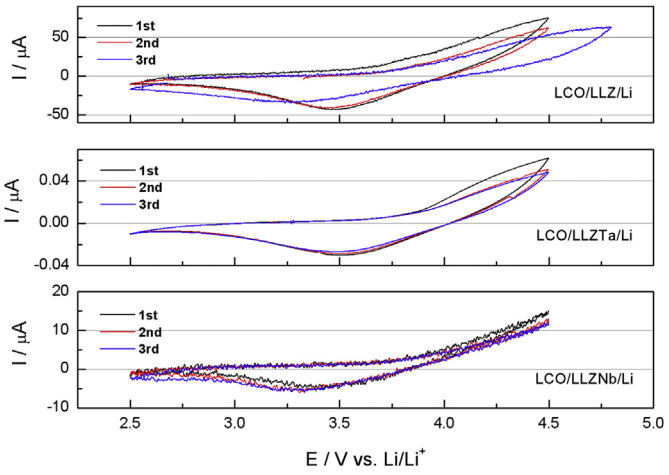

Fig. 10. Cyclic voltammetry tests of all-solid-state cells with solid electrolyte of LLZ, LLZTa and LLZNb at a scanning rate of 1 mV min^{-1}.

evaporate with longer sintering duration time, which could also decrease the conductivity.

Similarly, the effect of sintering duration time of Nb-doped LLZ was also investigated. The samples' conductivity after sintering with Al aid for different duration time was shown in Fig. 7. At 25 °C, the conductivity was enhanced to 4.11×10^{-4} S cm^{-1} for 12 h and 4.25×10^{-4} S cm^{-1} for 24 h, respectively. With increasing measurement temperature, the conductivities increased as expected, and came to a close value which was higher than 9×10^{-4} S cm^{-1}.

In addition to the sintering duration time, the doping content is another important factor which would greatly affect the conductivity. Thus, LLZ with different amount of Nb element was prepared to study the doping content effect. As can be seen in Fig. 8, the conductivity of Nb doped LLZ with Al aid was strongly dependent on the doping content. When the doping content was lower, with $Li_7La_3(Zr_{1.75}Nb_{0.25})O_{12}$ as the nominal formula, the conductivity at 25 °C was lower. But it was getting close to that of $Li_7La_3(Zr_{1.625}Nb_{0.375})O_{12}$ as the measuring temperature increased. The conductivity at 25 °C could be enhanced by more doping such as $Li_7La_3(Zr_{1.5}Nb_{0.5})O_{12}$, with a value of 4.50×10^{-4} S cm^{-1}. When measured at 50 °C, the conductivity of $Li_7La_3(Zr_{1.5}Nb_{0.5})O_{12}$ sample exhibited a conductivity as high as 1.23×10^{-3} S cm^{-1}.

3.2. All-solid-state cell performance

In all-solid-state cell configuration, LCO was used as the cathode material and Li metal as anode. LCO sol precursor was coated on LLZ pellet with the spin coating method followed by annealing in air. To check the availability of LCO crystal phase, Raman data were collected on the cathode side, as shown in Fig. 9. The square symbol marks the Raman peaks of LCO powder, which proves the formation of LCO crystal phase. The spectrum collected from the other side of LLZ pellet agreed with the cubic garnet structure, indicating no penetration of LCO sol.

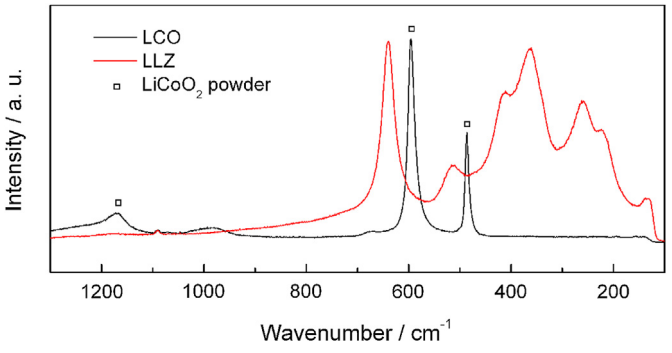

Fig. 9. Raman spectra of both surfaces of LLZ after spin coating of LCO and annealing.

The cyclic voltammetry curves of the all-solid-state cells with LLZ, LLZTa and LLZNb as electrolytes are shown in Fig. 10, respectively. The measurement was performed from 2.5 V to 4.5 or 5.0 V (vs. Li/Li^+) at a scanning rate of 1 mV min^{-1}. All the curves showed redox peaks at around 3.5 V, but it was a bit lower than 3.5 V in the case of LLZNb cell. The CV measurements indicated the successful working of these all-solid-state cells. However, the current was very low, especially for the cell with LLZTa electrolyte, which might be the result of the large resistance from the electrode/electrolyte interfaces.

4. Conclusions

LLZ solid electrolytes with Zr site substitution by Ta and Nb were prepared via the conventional solid-state reaction. After sintering at 1150 °C, Ta or Nb doping enhanced the conductivity by improving the micro-structure. The sintering duration time and doping content were optimized for Ta and Nb doping, with an enhanced conductivity at 25 °C of 4.09×10^{-4} S cm^{-1} and 4.50×10^{-4} S cm^{-1}, respectively. When measured at 50 °C, a high conductivity of 1.23×10^{-3} S cm^{-1} could be obtained with the optimized Nb-doped LLZ sample. All-solid-state cells with LLZ, LLZTa and LLZNb were fabricated and tested. LCO cathode was prepared on LLZ with spin coating followed by annealing, and the all-solid-state cells worked successfully evidenced by the redox peaks at around 3.5 V in CV measurements. However, more research on improving the electrode/electrolyte interface is needed, in order to obtain a better battery performance.

References

[1] P.G. Bruce, S.A. Freunberger, L.J. Hardwick, J.-M. Tarascon, Nat. Mater. 11 (2012) 19–29.
[2] B. Scrosati, J. Garche, J. Power Sources 195 (2010) 2419–2430.
[3] J.B. Goodenough, Y. Kim, Chem. Mater. 22 (2010) 587–603.
[4] J.W. Fergus, J. Power Sources 195 (2010) 4554–4569.
[5] P. Knauth, Solid State Ionics 180 (2009) 911–916.
[6] M. Kotobuki, K. Kanamura, Y. Sato, T. Yoshida, J. Power Sources 196 (2011) 7750–7754.

[7] K.H. Kim, Y. Iriyama, K. Yamamoto, S. Kumazaki, T. Asaka, K. Tanabe, C.A.J. Fisher, T. Hirayama, R. Murugan, Z. Ogumi, J. Power Sources 196 (2011) 764–767.
[8] M. Kotobuki, H. Munakata, K. Kanamura, Y. Sato, T. Yoshida, J. Electrochem Soc. 157 (2010) A1076–A1079.
[9] Y. Li, Y. Cao, X. Guo, Solid State Ionics 253 (2013) 76–80.
[10] E. Rangasamy, J. Wolfenstine, J. Sakamoto, Solid State Ionics 206 (2012) 28–32.
[11] M. Kotobuki, K. Kanamura, Y. Sato, K. Yamamoto, T. Yoshida, J. Power Sources 199 (2012) 346–349.
[12] M. Huang, T. Liu, Y. Deng, H. Geng, Y. Shen, Y. Lin, C.-W. Nan, Solid State Ionics 204–205 (2011) 41–45.
[13] M. Huang, A. Dumon, Y. Shen, C.-W. Nan, J. Chin. Ceram. Soc. 41 (2013) 1042–1045.
[14] R. Murugan, V. Thangadurai, W. Weppner, Angew. Chem. Int. Ed. 46 (2007) 7778–7781.
[15] E. Rangasamy, J. Wolfenstine, J. Allen, J. Sakamoto, J. Power Sources 230 (2013) 261–266.
[16] A. Dumon, M. Huang, Y. Shen, C.-W. Nan, Solid State Ionics 243 (2013) 36–41.
[17] M. Huang, A. Dumon, C.-W. Nan, Electrochem. Commun. 21 (2012) 62–64.
[18] J.L. Allen, J. Wolfenstine, E. Rangasamy, J. Sakamoto, J. Power Sources 206 (2012) 315–319.
[19] S. Ohta, T. Kobayashi, T. Asaoka, J. Power Sources 196 (2011) 3342–3345.
[20] Y. Jin, P.J. McGinn, J. Power Sources 196 (2011) 8683–8687.
[21] T.H. Rho, K. Kanamura, T. Umegaki, J. Electrochem. Soc. 150 (A107) (2003) A107–A111.